New Triple-Junction Solar Cell Assembly Process for Concentrator Photovoltaic Applications

Konan Kouame, P. Haghparast, Pierre Albert, Artur Turala, Thomas Bidaud, Abdelatif Jaouad, David Danovitch, Gwenaelle Hamon, Maïté Volatier, Vincent Aimez, et al.

New Triple-Junction Solar Cell Assembly Process for Concentrator Photovoltaic Applications.

Konan Kouame
LN2, 3IT
CNRS Université de Sherbrooke, Sherbrooke, Qc, Canada
konan.jean.herbert.kouame@usherbrooke.ca

P. Haghparast
LN2, 3IT
CNRS Université de Sherbrooke, Sherbrooke, Qc, Canada
payam.haghparast@usherbrooke.ca

Pierre Albert
LN2, 3IT
CNRS Université de Sherbrooke, Sherbrooke, Qc, Canada
pierre.albert@usherbrooke.ca

Artur Turala
LN2, 3IT
CNRS Université de Sherbrooke, Sherbrooke, Qc, Canada
artur.turala@usherbrooke.ca

Thomas Bidaud
LN2, 3IT
CNRS Université de Sherbrooke, Sherbrooke, Qc, Canada
thomas.bidaud@usherbrooke.ca

Abdelatif Jaouad
LN2, 3IT
CNRS Université de Sherbrooke, Sherbrooke, Qc, Canada
abdelatif.jaouad@usherbrooke.ca

David Danovitch
LN2, 3IT
CNRS Université de Sherbrooke, Sherbrooke, Qc, Canada
david.danovitch@usherbrooke.ca

Gwenaelle Hamon
LN2, 3IT
CNRS Université de Sherbrooke, Sherbrooke, Qc, Canada,
gwenaelle.hamon@usherbrooke.ca

Maïté Volatier
LN2, 3IT
CNRS Université de Sherbrooke, Sherbrooke, Qc, Canada
maite.volatier@usherbrooke.ca

Vincent Aimez
LN2, 3IT
CNRS Université de Sherbrooke, Sherbrooke, Qc, Canada
vincent.aimez@usherbrooke.ca

Maxime Darnon
LN2, 3IT
CNRS Université de Sherbrooke, Sherbrooke, Qc, Canada,
maxime.darnon@usherbrooke.ca

***Abstract*—We developed a new assembly process to fabricate concentrator photovoltaic (CPV) modules based on microelectronic surface mount technologies (SMT). Functional characterizations of resultant modules demonstrated that the configuration and process did not degrade solar cell performance. Dimensional characterizations showed high placement accuracy. The thermal performance was compared to a standard CPV module using ANSYS finite element thermal simulations. The SMT based module was shown to dissipate heat more efficiently than the conventional module with a device temperature of 58±0.24°C compared to 69±0.34°C. This proof of concept demonstrates viability of the new assembly process with a strong potential to reduce CPV integration costs.**

Keywords—photovoltaics, concentrator photovoltaic, CPV, surface mount technologies, SMT, thermal simulation, finite elements, solar cell assembly

I. INTRODUCTION

Concentrator Photovoltaics (CPV) is a solar electricity production technology. Using concentrated incident sunlight onto a high efficiency solar cell, this approach holds the record for solar energy conversion efficiency (47.6%) using a 6-junction solar cell [1]. However, this technology remains less competitive than crystalline silicon-based photovoltaics due to materials cost and technology complexity. The Levelized Cost of Energy (LCOE) is the accepted metric in determining the potential commercialization of a photovoltaic technology. It characterizes the return on investment by considering parameters such as lifetime, initial cost, and maintenance of a photovoltaic panel. One means to reduce CPV LCOE is to simplify the assembly process. Another is to increase module lifetime by, for example, reducing the solar cell operating temperature. Indeed, the high concentration of incident light onto CPV solar cells implies a significant amount of converted heat that, if not dissipated, can lead to drastic deterioration of the cell. In the literature [2-4], cell suppliers generally advise users to maintain cells at temperatures below 100°C-120°C. However, Espinet-González *et al.* [5] showed that an operating temperature above 80°C can significantly deteriorate the cells reliability. Achieving an operating temperature below 80 °C demands a particular attention to the thermal path while at the same time avoiding cost-prohibitive solutions. As such, a passive dissipation technology with a heat sink is preferred overactive cooling [6].

Considering these issues, we propose a new assembly process for CPV modules based on surface mount technologies (SMT) used in microelectronics. Specifically, we exploit flip chip or C4 (Controlled Collapse Chip Connexion) technology as originally invented by IBM [7]. This manufacturing process eliminates the need for wire bonding, thus reducing module assembly time while providing high alignment accuracy (≤ 25µm), and improved heat dissipation. While several new CPV module configurations [8-10] propose similar SMT approaches, they use non-standard solar cells *i.e.*, solar cells with the two (+) and (-) contacts on one side of the cell only. The SMT process presented here enables the use of more cost effective standard solar cells comprising one contact on each side and can be applied to both macro CPV (solar cell size > 1 mm^2) and micro CPV (solar cell size ≤ 1 mm^2).

In this paper, we first propose and develop an SMT assembly process for standard triple-junction III-V/Ge solar cells on glass

substrates. The assembled solar cells are then characterized in the laboratory (indoor characterization). Finally, a thermal simulation is performed to compare the thermal performances of the two assembly configurations, *i.e.*, a standard configuration based on wire bonding and the proposed SMT flip chip configuration.

II. Development of the Assembly Process

We used hexagonal triple junction solar cells as shown in Fig. 2-a. Based on the cell design, we designed and fabricated a glass PCB, shown in Fig. 2-b, in our laboratory.

The proposed process is summarized in Fig. 1. The different stages and their development are as follows:

1- The glass used is a microscope glass slide. The glass substrate is cleaned by solvent followed by O_2 plasma cleaning (15 min) to remove any organic compounds from the substrate.

2- The resdistribution lines (RDL) are formed by lithography and lift-off processes. The metal stack used here is composed of Cr/Cu/Ni/Au of 20/1200/50/5nm thicknesses, respectively, and was deposited by sputtering. Cr ensures good adhesion to the

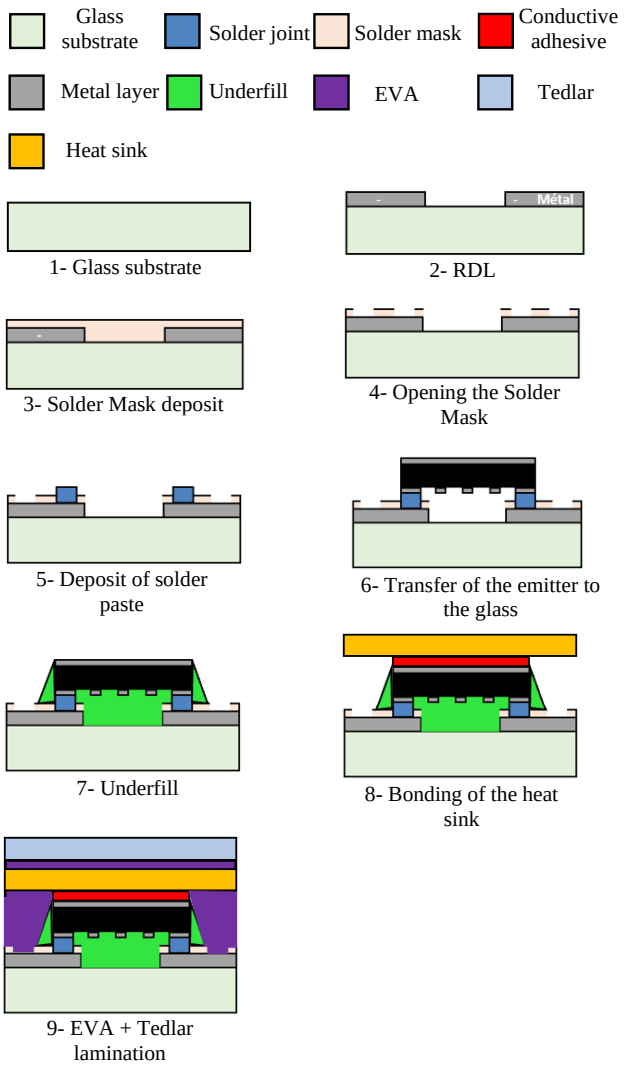

Fig. 1. Process flow of solar cell assembly on glass substrate.

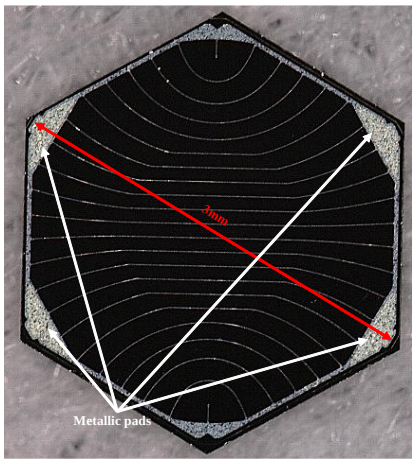

a- Hexagonal III-V/Ge Solar Cell

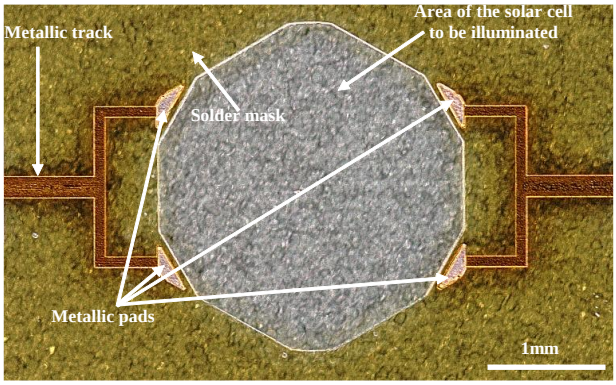

b- Example of glass PCB

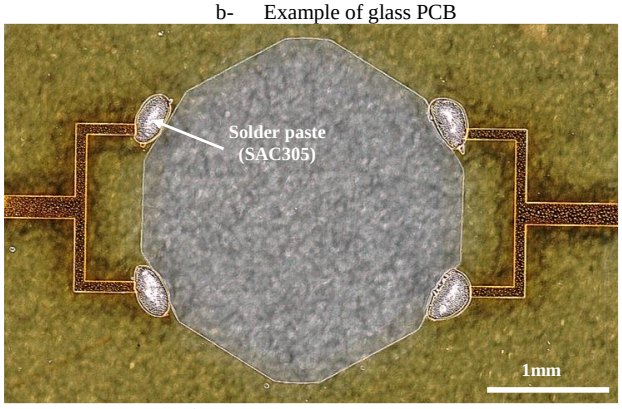

c- Local deposit of solder paste by stencil printing on glass PCB.

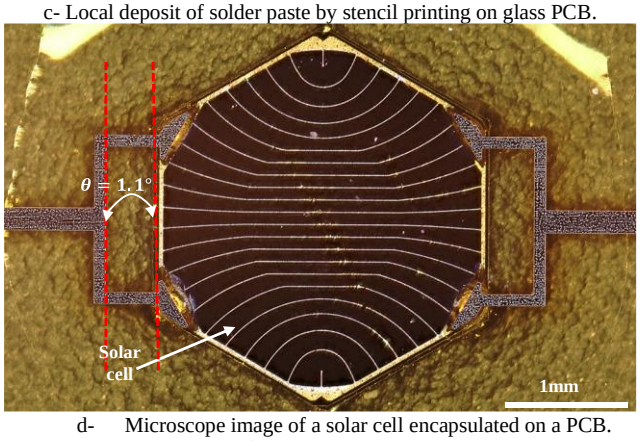

d- Microscope image of a solar cell encapsulated on a PCB.

Fig. 2: Microscope images of hexagonal solar cell, glass PCB, solder paste deposition, cell soldered and underfilling.

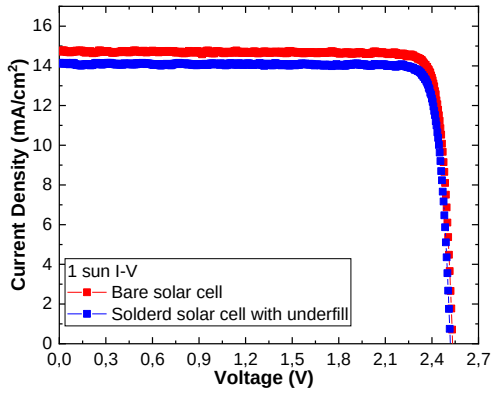

Fig. 3. I-V characteristics of bare and encapsulated solar cells measured under 1 sun (AM1.5D) illumination.

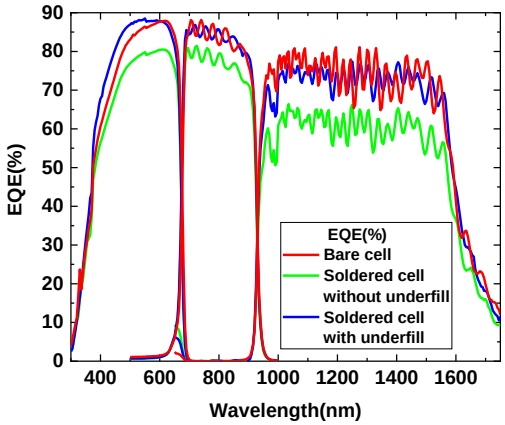

Fig. 4. EQE measurements of bare hexagonal solar cells (red), soldered hexagonal solar cell without underfill (green) and soldered hexagonal solar cell with underfill (blue).

glass and the connection track, the latter being of Cu to promote high current flow between assembled components. Nickel serves as a diffusion barrier layer between the Cu tracks and the SnAgCu based solder alloy known as SAC305, thus avoiding excessive formation of brittle Cu-Sn intermetallics. The thin Au prevents Ni oxidation, thus optimizing wetting of the solder alloy. We observed no delamination after metal deposition on the glass substrate. The solder areas and the active area of the solar cell are defined by photolithography.

3- A 5 µm-thick HD4104 photosensitive polyimide is deposited as a solder mask by spin coating.

4- The solder mask is patterned by UV lithography. A curing of polyimide in the presence of nitrogen 200 °C / 30 min (rate 10 °C / min) followed by 375 °C / 60min (rate 10°C/min) is performed. Located outside the illumination area, the solder mask limits solder to a restricted region that ensures sufficient solder height and therefore chip-substrate gap for subsequent underfill efficiency.

5- After the glass PCB manufacturing, the solder paste is locally deposited by stencil printing as shown in Fig. 2-c. An important aspect for the success of stencil printing is the area ratio. It is calculated for rectangular openings as follows:

$$area\ ratio = \frac{area\ opening}{area\ walls} = \frac{L * W}{2 * t * (L + W)}$$

where L is the length of the opening, W the width of the opening, and t the thickness of the stencil. The IPC 7525 industry standard recommends an area ratio greater than 0.66 to avoid stencil clogging [11]. The SAC305 solder paste was printed using an LPKF Protoprint manual tool. The stencil used is a Kapton sheet whose openings were made by laser cutting. The opening of the stencil and its thickness control the volume of solder paste deposited. For our study, 3 mil (76.2 µm) thick stencils were used. The area ratio was 0.96, thereby respecting the constraint mentioned above. The obtained solder paste thicknesses correlated to stencil thicknesses within a variation of $\pm$11 µm.

6- After the solder paste deposition on the glass PCB, the cell is assembled face down (active surface in front of the glass plate) using a Tresky 8800 chip pick and place tool. The solder is then reflowed using an LPKF Protoflow mass reflow oven. The reflow profile comprised a preheating zone of 170 °C / 170 s, a melting zone of 280 °C peak and 125 s time above liquidus (TAL) and a cooling zone from liquidus to room air for 110 s. The solar cells were placed with good accuracy and with rotation of less than 1.1°.

7- The last step is to fill the gap between the solar cell and the glass PCB using capillary dispensed underfill. We used Epotek transparent underfill contained in a syringe. A few droplets are deposited on the glass directly adjacent to the edge of the previously soldered solar cell. The underfill penetrates the gap between the cell and the glass (76.2 µm $\pm$ 11 µm) by capillary flow. The underfill is cured at 80°C for 3h. As visible in Fig. 2-d depicting the resultant assembly, the active area of the solar cell is free from bubbles or voids following underfill cure.

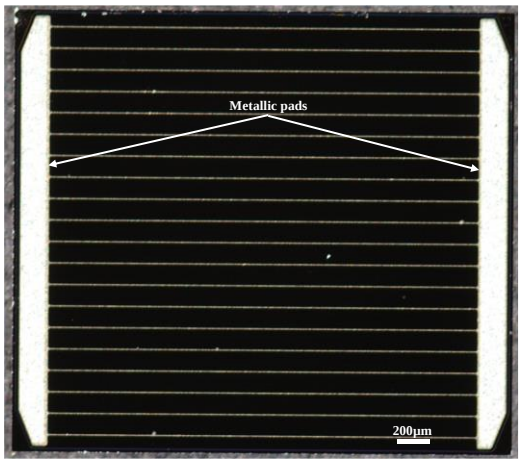

Fig. 5. Square III-V/Ge solar cell.

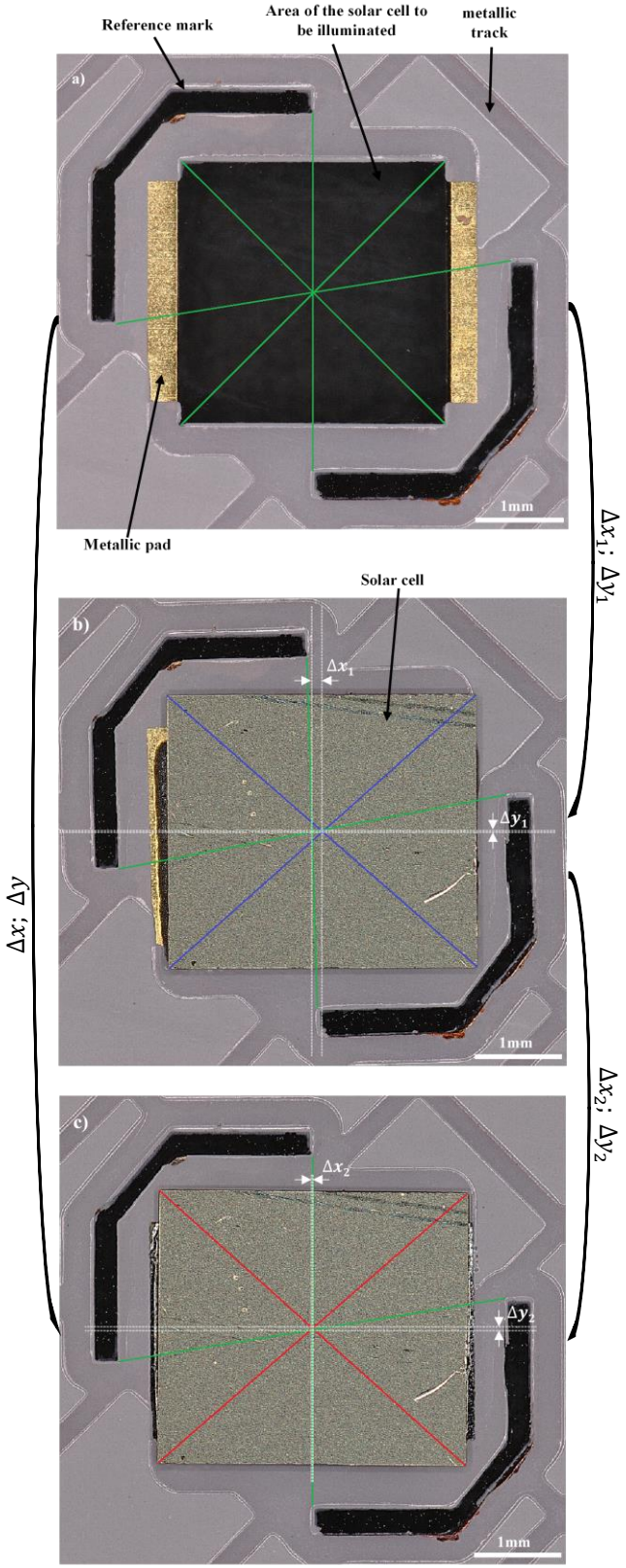

Fig. 6. Calculation method of Δx and Δy alignment of solar cells after assembly. a- Position of the PCB Center, b- Measurements of Δx_1 and Δy_1 from the positions of the center of the PCB and center of the solar cell after pick and place of the solar cell, c- Measurements of Δx_2 and Δy_2 from the positions of the PCB center and solar cell center after reflowing.

Steps 8 and 9, namely the heat sink bonding and the lamination of protective layers, were not developed at the time of publication. These last two steps are well mastered in the field of photovoltaics and therefore do not detract from the demonstration of our proof of concept.

III. Characterisation of the Assembly Process

To validate the success of the assembly, we performed both functional and dimensional characterisations. Current-voltage (I-V) measurements under simulated sunlight (AM1.5D) illumination determined the open circuit voltage (V_{OC}) and the fill factor (*FF*) which are important parameters of a solar cell. The quantum efficiency was obtained by the ratio of the number of carriers collected by the solar cell to the number of incident photons on the solar cell.

Fig. 3 shows the I-V characteristics of the bare and assembled solar cells. We obtained a *Voc* of 2.53V and a FF of 89.5% for both the bare and encapsulated solar cells. This confirms that the encapsulation process does not degrade the solar cells.

Fig. 4 shows the EQE of the bare solar cell, the soldered solar cell without underfill and the soldered solar cell with underfill. We observed a decrease in EQE for the soldered cell without underfill. This decrease is due to the light reflection at the air/glass, glass/air and air/cell interfaces. The addition of underfill reduces these reflections by allowing a good optical index matching at the different interfaces. Indeed, the index matching results mostly in an increase of the EQE after

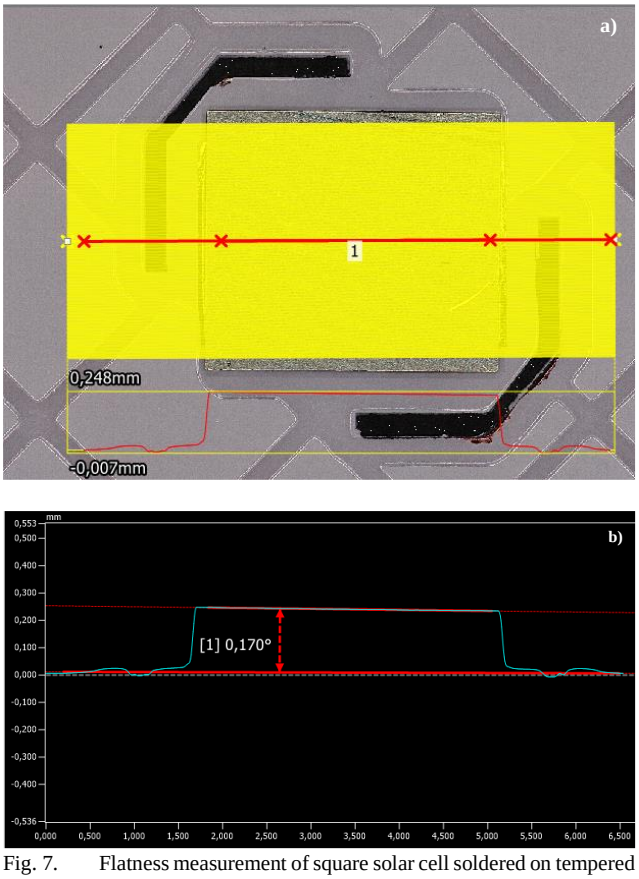

Fig. 7. Flatness measurement of square solar cell soldered on tempered glass.

underfilling. A slight decrease of the EQE is observed for the short wavelength (<600 nm) and is attributed to absorption of light at this wavelength by both the underfill and glass substrate.

To quantify the alignment accuracy in *x* and *y* axes and the flatness of the solar cell after assembly, we designed a second glass PCB with alignment marks and used rectangular solar cells as shown in Fig. 5. This cell comprises two quasi-rectangular-shape bus bars on each side. A brief description of the starting PCB is shown in Fig. 6-a, indicating a reference mark, the solder pads, the metal tracks and the area of the cell to be illuminated. The center of the PCB can be determined using the lines joining the reference marks and drawing diagonals through the area of the cell to be illuminated. Fig. 6-b shows the solar cell placed by pick and place on the PCB. The center of the cell and the center of the PCB are determined by drawing the diagonals of the solar cell in purple and the green lines joining the reference marks, respectively. The distances between the center of the solar cell and the center of the PCB in *x* and *y* axes are called Δx_1 and Δy_1 and are equal to 89 µm and 18 µm, respectively. Fig. 6-c shows the solar cells assembled on the glass PCB after reflowing in the reflow oven. Again, the cell and PCB centers are determined by the same method. The distances between the center of the solar cell and the center of the PCB in *x* and *y* are called Δx_2 and Δy_2 and are equal to -85 µm and 16 µm, respectively. The final misalignments Δx and Δy after assembly are calculated as the sum of $\Delta x_1 + \Delta x_2$ and $\Delta y_1 + \Delta y_2$ and are equal to 4 µm and 38 µm, respectively. We can notice that $\Delta x < \Delta x_1$ after reflowing and $\Delta y > \Delta y_1$ after reflowing. The reduction of Δx after reflowing is obtained as a result of the surface tension which realigns the solar cells during the mass reflow. The increase in Δy after reflowing is attributed to a dimensional mismatch between the solar cell and the PCB pads in the *y* axis, as shown in Fig. 5 and Fig. 6-a. As such, we expect that a well-matched design of the solar cells and PCB pads would lead to a similar placement accuracy in the *x* and *y* direction, i.e., around 4 µm.

Flatness was measured using a mechanical profilometer to scan 190 lines, with 7 µm line-to-line spacing, spanning both the glass PCB and the backside of the solar cell soldered to said PCB, as shown in Fig. 7-a. The average profile from these lines is shown in Fig. 7-b. The tilt obtained is 0.2°.

One prototype was cross-sectioned and observed by optical microscopy to determine the morphology of the underfill filet (see Fig. 8). We can see that the fillet spans the entire sidewall of the solar cell and extends horizontally on the PCB side by more than 1.15 mm. This shape is expected to provide good mechanical strength to the solar cell after soldering and the fact to have underfill on the wall avoid electrical shorting of the solar cell during the subsequent steps of module fabrication. Finally, no underfill residue was observed on the solar cell back side. Avoiding such residue is critical to optimal thermal dissipation between the solar cell and its heat sink.

IV. Thermal Performance Evaluation by Finite Element Modeling

We performed a finite element thermal simulation using ANSYS software to compare the thermal performance of

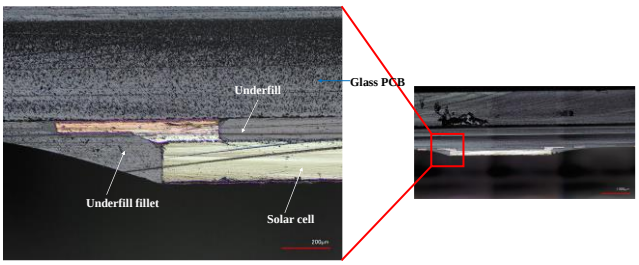

Fig. 8. Cross section microscope image of a solar cell packaged on glass.

commercial CPV modules to the CPV module using the SMT method developed in this project. The standard CPV model simulated here is based on the CPV module from STACE described in Fig. 9-a. In this model, the 3.4×3×0.18 mm^3 solar cell is attached to an aluminum die bond pad of size 7.25×4.5 mm and thickness 0.8 mm using conductive epoxy. The die bond pad is attached to the aluminum alloy heat sink by laser welding. The aluminum heat sink is 41×41 mm^2 size and 0.5 mm thick. The heat sink is glued to the glass plate, which is 2.7 mm-thick, and 57.143×57.143 mm^2 size. The glue used to glue the heat sink to the glass is insulating with a negligible thickness.

The CPV model using SMT is based on the one described in Part II. In the simulation model, a solar cell of size 3.4×3.0 mm^2 and thickness 180 µm is soldered onto a glass PCB measuring 57.143×57.143 mm^2, corresponding to the size of the lens, and a thickness of 2 mm. The metal tracks of the PCB are made of 35 µm-thick copper. The solder joints connecting the solar cell on the PCB measure 2.49×0.2 mm^2, and are 75 µm, thick. The resultant 75 µm gap between solar cell and PCB is filled with underfill. An underfill fillet of 1.15 mm length has also been added to the model as shown in Fig. 9-b. The backside of the solar cell is soldered to a heatsink of size 41×41mm^2 and thickness 0.5 mm. EVA (Ethylene Vinyl Acetate) encapsulant was used to fill any empty space in the package. The thickness of the EVA on the heatsink is 0.35 mm. A Tedlar backsheet of size 57.143×57.143 mm and thickness 0.2 mm is glued onto the encapsulant.

The materials and their thermal conductivities are provided in table 1. The III-V/Ge solar cell is considered as germanium chip because III-V material thickness is very small (~10 µm) compared to the Germanium thickness (~170 µm).

The simulations are performed for lenses with a concentration factor C_{geo} of 363×, *i.e.*, the lens concentrates 363 times the direct normal irradiance (*DNI*) on the solar cell. The

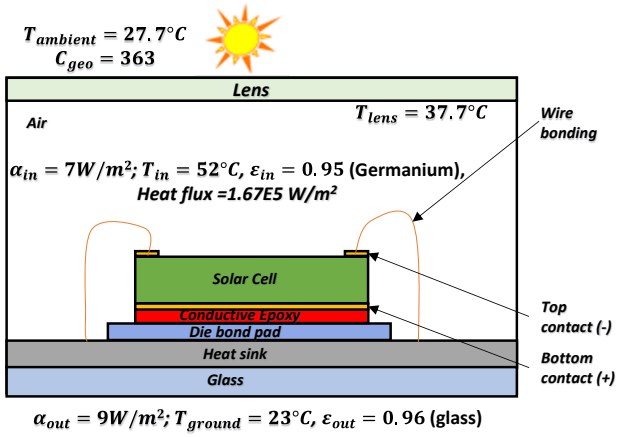

Fig. 9-a. Cross-sectional models of standard CPV modules simulate by finite element.

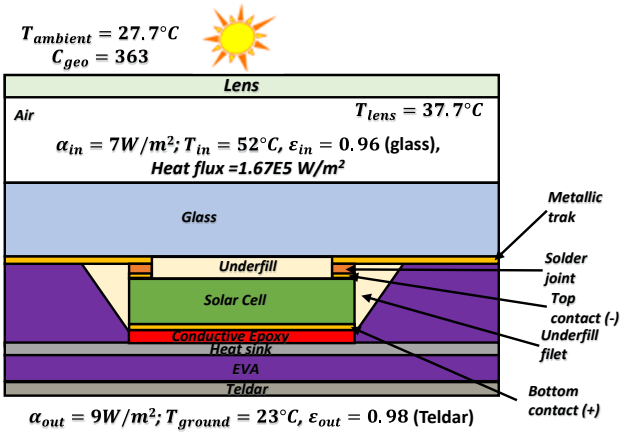

Fig. 9-b. Cross-sectional model of CPV module using SMT simulate by finite element.

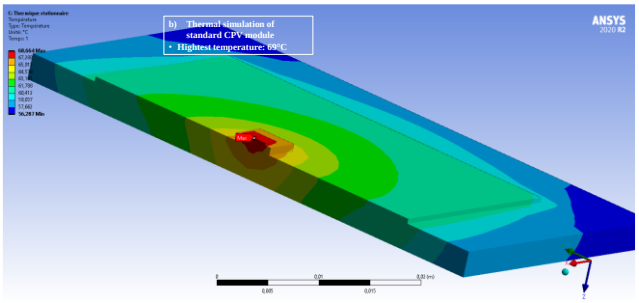

Fig. 10-a. Finite element simulation of standard CPV module showing 69°C.

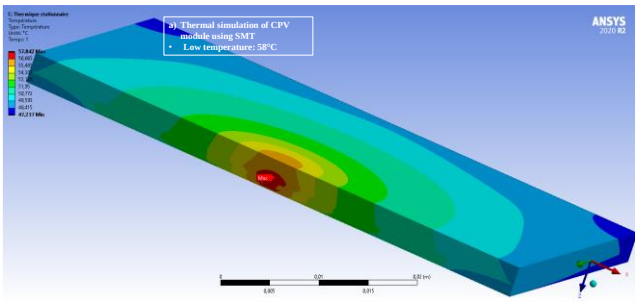

Fig. 10-b. Finite element simulation of CPV module using SMT showing 58°C.

optical efficiency is η_{opt} is 0.85 (*i.e.*, 85% of the DNI reaches the solar cell) and *DNI* on the lens is set to $900W/m^2$. The efficiency of the solar cells η_{cell} is set to 0.4 (*i.e.* 40% of the light received by the solar cell is converted into electricity and the rest is converted into heat). The heat flux to be dissipated $q_{th,in,Pmpp}$ is calculated as follows:

$$q_{th,in,Pmpp} = C_{geo} * DNI * \eta_{opt} * A_{cell} * (1 - \eta_{cell})$$

where A_{cell} is the cell area.

TABLE I. MATERIALS AND THERMAL CONDUCTIVITY OF EACH LAYER OF BOTH CPV MODULES [15,16]

Layer of CPV module	Material	Isotropic thermal conductivity (W/m.K)	
Glass PCB	Tempered	1.8	
Metallic track	Copper	399	
Solder joint	SAC305	60	
Underfill	Sylgard 184	0.27	
Solar cell	Germanium	60	
Heat sink	Aluminium alloy	173.15K	114
		273.15K	144
		373.15K	165
		473.15K	175
Backsheet	EVA	0.35	
	Teldar	0.2	
Die bond pad	Aluminium alloy		
Conductive adhesive	Conductive epoxy	85	

TABLE II. CONVECTION AND EMISSIVITY COEFFICIENTS

Convection coefficient (α)	$\alpha_{out} = 9W/(m^2.K)$
	$\alpha_{in} = 7W/(m^2.K)$
Emissivity coefficient (ε)	$\varepsilon_{Teldar} = 0.96$
	$\varepsilon_{Glass} = 0.3$
	$\varepsilon_{metal} = 0.3$
Temperature	$T_{ambient} = 27.7°C$
	$T_{in} = 52°C$
	$T_{ground} = 23°C$
	$T_{lens} = 37.5°C$

There are 3 modes of heat transfer in a CPV module: radiation, convection, and conduction. The module exchanges heat with the environment by radiation and convection. The coefficients of these heat exchanges are obtained from the literature [12-14] and are recalled in table 2. Thermal conduction is governed by the thermal conductivity of the materials in contact within the package. Wire bonding thermal conduction is considered to be neglectible and is not included in the simulation model of the standard CPV module.

The results obtained are presented in Fig. 10-a and Fig. 10-b. The thermal finite element simulations show that the maximum temperature of the standard CPV module is 69°C while that of the CPV module using SMT is 58°C. Therefore, for the same boundary conditions, solar cell type and heat sink type, a lower temperature is obtained in the CPV module using the SMT configuration. It is proposed that the solar cell in the SMT module, being located below the glass, is not directly exposed to the warm air inside the solar module, thereby facilitating its heat dissipation. This lower cell temperature is expected to improve both the module efficiency and its lifetime.

V. Conclusion

An SMT (flip chip) assembly process of a solar cell onto a glass PCB has been proposed and developed. The solar cell thus packaged has been characterized under AM1.5D illumination. Measurements show that the soldering process does not degrade the cell performance. The underfilling of the gap between the solar cell and the PCB by a transparent material is achieved without the presence of bubbles or voids at the cell-glass interface. This underfilling ensures minimal light reflection at the different interfaces. Alignment accuracies of 4, 34 µm and 0.2° are obtained in the *x*, *y* and *theta* directions respectively after soldering. Finite element thermal simulation results also show that the module using SMT dissipates heat more effectively than the Standard module under the same simulation conditions with maximum temperatures being 58°C and 69°C, respectively.

It is therefore expected that the proposed SMT configuration and assembly method will enable accurate placement of high efficiency solar cells while reducing both assembly process complexity and cell operating temperature, thus promising to reduce the cost of concentrator photovoltaic technologies.

Acknowledgment

We acknowledge the support from STACE, NSERC and Prompt, for their material and financial support in the MARS-CPV project. LN2 is a joint International Research Laboratory (IRL 3463) funded and co-operated in Canada by Université de Sherbrooke (UdeS) and in France by CNRS as well as ECL, INSA Lyon, and Université Grenoble Alpes (UGA).

References

[1] M. A. Green, E. D. Dunlop, G. Siefer, M. Yoshita, N. Kopidakis, K. Bothe and X. Hao, "Solar cell efficiency tables (Version 61)", Progress in photovoltaics, 2022.

[2] AZURSPACE solar power GmbH, Concentrator triple junction solar cell-type 3C42 data sheet, 2014. ⟨http://www.azurspace.com/images/pdfs/DB_3879-00-00_3C42_AzurDesign_3x3_20140226.pdf⟩ (accessed 22.01.2023).

[3] Spectrolab Inc., CPV point focus solar cells–type C3MJ Data sheet, 2011. ⟨https://www.spectrolab.com/photovoltaics/C4MJ_40_Percent_Solar_Cell.pdf⟩ (accessed 22.01.2023).

[4] G. Segev, G. Mittelman, A. Kribus, Equivalent circuit models for triple-junction concentrator solar cells, Sol. Energy Mater. Sol. Cells 98 (2012) 57–65, http://dx.doi.org/10.1016/j.solmat.2011.10.013.

[5] P. Espinet-González, C. Algora, N. Núñez, V. Orlando, M. Vázquez, J. Bautista, et al., Temperature accelerated life test on commercial concentrator III–V triple-junction solar cells and reliability analysis as a function of the operating temperature, Prog. Photovolt. Res. Appl. 23 (2015) 559–569, http://dx.doi.org/10.1002/pip.2461.

[6] Manxuan Xiao, Llewellyn Tang, Xingxing Zhang 3, Isaac Yu Fat Lun and Yanping Yuan, "A Review on Recent Development of CoolingTechnologies for Concentrated Photovoltaics(CPV) Systems," Published: 6 December 2018

[7] L.F. Miller, "Controlled Collapse Reflow Chip Joining," IBM J. Res. Develop., v.13, p.239, 1969.

[8] S. Burroughs et al., "A New Approach For A Low Cost CPV Module Design Utilizing MicroTransfer Printing Technology," Freiburg, (Germany), 2010, pp. 163–166, doi: 10.1063/1.3509179.

[9] K. Ghosal, B. Fisher, D. Lilly, J. Gabriel, S. Seel, and S. Burroughs, "Ultrahigh Efficiency HCPV Modules and Systems," IEEE Journal of Photovoltaics, vol. 6, no. 5, pp. 1360–1365, Sep. 2016, doi: 10.1109/JPHOTOV.2016.2590884.

[10] T. Nakagawa et al., "High-efficiency Thin and Compact Concentrator Photovoltaics with Micro-solar Cells Directly Attached to Lens Array," in Light, Energy and the Environment, Canberra, 2014, p. RF4B.5, doi: 10.1364/OSE.2014.RF4B.5.18.

[11] Subrat Prajapati, "Design Guidelines for Stencil Design using Regression", IPC-7525A: Stencil Design Guidelines, Larsen & Toubro Limited, Mysore, Karnataka, (India).

[12] J. C. Jaus, Entwicklung von photovoltaischen Konzentratormodulen mit Fresnel-Linsen und reflektiver Sekundäroptik, Dissertation, Albert-Ludwigs-Universität, 2009.

[13] J. Jaus, R. Hue, M. Wiesenfarth, G. Peharz, and A. W. Bett, "Thermal management in a passively cooled concentrator photovoltaic module," in Proceedings of the 23rd European.

[14] Maike Wiesenfarth, Dimitre Iankov, Juan F. Martínez, Peter Nitz, Marc Steiner, Frank Dimroth and Henning Helmers, "Technical Boundaries of Micro-CPV Module Components: How Small is Enough,?" Fraunhofer Institute for Solar Energy Systems ISE, Freiburg, (Germany), AIP Conference Proceedings 2550, 030008 (2022); https://doi.org/10.1063/5.0099878 Published Online: 02 September 2022.

[15] Tsung-Lin Chou, Zun-Hao Shih, Hwen-Fen Hong, Cheng-Nan Han, and Kou-Ning Chiang, "Thermal Performance Assessment and Validation of High-Concentration Photovoltaic Solar Cell Module," IEEE Transactions on Components, Packaging and Manufacturing Technology, VOL. 2, NO. 4, APRIL 2012.

[16] Nan Jiang, Abdol Ghaffar Ebadi, Kakarla Hari Kishore, Qahtan. A. Yousif, Mohammad Salmani, "Thermomechanical Reliability Assessment of Solder Joints in a Photovoltaic Module Operated in a Hot Climate," DOI 10.1109/TCPMT.2019.2933057, IEEE Transactions on Components, Packaging and Manufacturing Technology.